Smooth real-time motion planning based on a cascade dual-quaternion screw-geometry MPC

Ainoor Teimoorzadeh, Frederico Fernandes Afonso Silva, Luis F.C. Figueredo
and Sami Haddadin

Chair of Robotics and Systems Intelligence,
Munich Institute of Robotics and Machine Intelligence,
Technical University of Munich, DE-80992 Munich, Germany,
`ainoor.teimoorzadeh@tum.de`

Abstract. This paper investigates the tracking problem of a smooth coordinate-invariant trajectory using dual quaternion algebra. The proposed architecture consists of a cascade structure in which the outer-loop MPC performs real-time smoothing of the manipulator's end-effector twist while an inner-loop kinematic controller ensures tracking of the instantaneous desired end-effector pose. Experiments on a 7-DoF Franka Emika Panda robotic manipulator validate the proposed method demonstrating its application to constraint the robot twists, accelerations and jerks within prescribed bounds.

1   INTRODUCTION

Robotic manipulators are gaining broad acceptance in a wide range of applications, varying from manufacturing to assistive care. As the robotic applications of serial manipulators grow, so does the complexity of the environment and the conditions in which they operate. This brings extra challenges into the planning and control formulation, as constraints on the end-effector should be satisfied during motion. For instance, carrying a bottle of water may require holding the cup straight while allowing free motion in the Cartesian space—regardless of the reference frame used to describe the motion, e.g., reference frame from a camera or robot base. Furthermore, when sharing the environment with humans, the robot should prioritize coordinate invariant, easy to demonstrate and real-time smooth movements, while ensuring the imposition of safety constraints [1–4].

To address this challenge, this work proposes a reactive planning approach based on the sate-of-the-art coordinate-invariant real-time path planning. The approach is built on the screw geometry of motion along side a model-predictive control and kinodynamic constraints in the task space. Separately, screw motion and model-predictive control are well-developed areas within the control and robotics communities. The former has been largely studied with a multitude of applications [5–16], and more recently integrated into real-time path planning approaches given its coordinate invariance properties [17–19], whereas the latter has experienced a surge of results in the past decades, particularly within field-robotics [20]. Nevertheless, only a few studies have explored solutions falling in the intersection of both fields, and to the best of the authors' knowledge, none have been shown to satisfy the inherent translation and rotation coupling

that describes rigid body motions in SE(3), as well as screw geometry with constraint and coordinate-invariance properties necessary for real-world constraint satisfaction.

Reactive motion and path planners for real-world applications often rely on dynamics or control systems with convergence and stabilization properties, such as [21, 22], or on geometric constraint satisfaction through interpolation methods [23]. Although the former provides stabilization features and allows for kinodynamic planning, they often lack formal guarantees to satisfy geometric constraints and have poor explainability of the resulting trajectory, which is only locally optimized. In contrast, interpolation approaches are easy to deploy, interpret, and generalize from demonstrations; that is, a simple demonstration can be used to guide a path planner, as seen in [23]. Therefore, they are often preferred in industry and service robotics. However, care must be taken to ensure a proper group structure when performing interpolation and addressing the geometric constraints. Several results still decouple translation and rotation components—and some even consider Euler angles, which are widely known to be singular and non-representative for motions—which lead to poor results and dependency on the reference frame.[1] Readers are referred to [19, 24–26]. In this study, our planner produces paths through screw linear interpolation (ScLERP) [25] that implicitly maps—and therefore satisfies—all geometric constraints embedded in the single demonstration.

Notwithstanding, defining smooth continuous, C_1 or C_2 trajectories through demonstration or interpolation whilst satisfying the inherent geometric constraints is not trivial. As one includes additional velocity and acceleration constraints, following the trajectory and keypoints becomes challenging. Allmendinger et al. [24] proposes a parameter selection for a dual-quaternion C_1 screw linear interpolation but the approach is fairly limited to special cases. In contrast, recent quadratic-programming and model-predictive control solutions are well-suited to ensure constraint satisfaction with fewer parameters. Particularly, model predictive control (MPC) formulations allow the control of constrained multiple-input multiple-output nonlinear systems with respect to an optimal criteria. Similarly to H_2 and H_∞ strategies [27] and to quadratic-programming-based controllers [28], MPC approaches explore the solution of an optimal control problem. However, differently from the former, MPCs have a finite time horizon that enables the online solution of the optimal control problem [29, 30], making it suitable for dynamic trajectory tracking within cluttered environments [31]. The ongoing advancements in the underlying theoretical framework has evolved MPC into a reliable control technique capable of offering stable, robust, constraint-compliant controllers, and computationally feasible solutions for both linear and nonlinear systems [32]. Moreover, the predictive capability of MPCs lead to enhanced trajectory tracking performance by effectively handling disturbances and generating smooth control signals [29]. However, most approaches have a decoupled treatment of the translational and rotational components of the mechanism [33]. Thus, increasing the number of equations, the overall complexity

---

[1] Coordinate invariance should always be addressed. Otherwise, one may even have different results in trajectory tracking simply by changing features within an object topology, e.g., visual tracking of different edges in a mesh or a point cloud.

of the system, and often leading to the reference-frame dependency. For instance, Pereira et al. [30] used a $SE(3)$ representation of a quadrotor UAV and of the obstacles present in a cluttered environment. Based on that, the authors proposed a nonlinear model predictive control strategy for the execution of aggressive maneuvers. However, albeit free from the representation singularities inherent from the extraction of Euler angles from rotation matrices, both the dynamic model of the UAV and the control formulation present decoupled equations for the attitude and the position of the system, given in $SO(3)$ and in $\mathbb{R}^3$, respectively.

This paper presents the integration of a screw-interpolation strategy that satisfies path and geometric constraints within a coordinate-invariant manner with a dual-quaternion algebra MPC that constraints twists, accelerations and jerks within prescribed bounds. Dual quaternions provide a unified representation of the angular and linear components with strong geometrical meaning while being free of representational singularities, more compact, and having lower computational costs than homogeneous transformation matrices [34]. The proposed architecture is a cascade structure in which the outer-most MPC controller smooths the coordinate-invariant trajectory of the end-effector twist in real-time while the inner-loop kinematic controller ensures tracking of the instantaneous desired end-effector pose.

We validate the proposed method in experiments on a 7-DoF Franka Emika Panda robotic manipulator including constraints on the robot twists, accelerations and jerks within prescribed bounds.

2 Problem Formulation

In this section, we provide an overview of the definitions and fundamentals of the planning problem. Firstly, we review the core concepts related to the algebra of dual quaternions (DQ) and the properties of a screw-linear theory based first-order interpolation. These will build the backbone of the proposed planning scheme.

2.1 Mathematical Preliminaries

Dual quaternions [35] are elements of the set

$$\mathcal{H} \triangleq \{ \boldsymbol{h}_\mathcal{P} + \varepsilon \boldsymbol{h}_\mathcal{D} : \boldsymbol{h}_\mathcal{P}, \boldsymbol{h}_\mathcal{D} \in \mathbb{H},\, \varepsilon \neq 0,\, \varepsilon^2 = 0 \},$$

where $\mathbb{H} \triangleq \{ h_1 + \hat{\imath} h_2 + \hat{\jmath} h_3 + \hat{k} h_4 \,:\, h_1, h_2, h_3, h_4 \in \mathbb{R} \}$ is the set of quaternions, in which $\hat{\imath}$, $\hat{\jmath}$ and $\hat{k}$ are imaginary units with the properties $\hat{\imath}^2 = \hat{\jmath}^2 = \hat{k}^2 = \hat{\imath}\hat{\jmath}\hat{k} = -1$ [35]. Addition and multiplication of dual quaternions are analogous to their counterparts of real and complex numbers. One must only respect the properties of the dual unit ε and imaginary units $\hat{\imath}, \hat{\jmath}, \hat{k}$.

The subset $\underline{\boldsymbol{\mathcal{S}}} = \{ \underline{\boldsymbol{h}} \in \mathcal{H} : \|\underline{\boldsymbol{h}}\| = 1 \}$ is the subset of unit dual quaternions, where $\|\underline{\boldsymbol{h}}\| = \sqrt{\underline{\boldsymbol{h}}\underline{\boldsymbol{h}}^*} = \sqrt{\underline{\boldsymbol{h}}^*\underline{\boldsymbol{h}}}$, with $\underline{\boldsymbol{h}}^*$ being the conjugate of $\underline{\boldsymbol{h}}$ [36]. Under the multiplication operation, this subset defines the group $\mathrm{Spin}(3) \ltimes \mathbb{R}^3$ which double covers $SE(3)$ [35]. Any arbitrary rigid body transformation can be represented by the unit dual quaternion $\underline{\boldsymbol{x}} \in \mathrm{Spin}(3) \ltimes \mathbb{R}^3$,

$$\underline{\boldsymbol{x}} = \boldsymbol{r} + \varepsilon \left(1/2 \right) \boldsymbol{p} \boldsymbol{r}, \tag{1}$$

where $\boldsymbol{p} = \hat{\imath}x + \hat{\jmath}y + \hat{k}z \in \mathbb{H}_p$ represents the Cartesian position (x, y, z) within the set of pure quaternions, i.e., $\mathbb{H}_p \triangleq \{\boldsymbol{h} \in \mathbb{H} : \mathrm{Re}\,(\boldsymbol{h}) = 0\}$, where the real component is null, i.e., $\mathrm{Re}\left(h_1 + \hat{\imath}h_2 + \hat{\jmath}h_3 + \hat{k}h_4\right) \triangleq h_1$. The rotation $\boldsymbol{r} = \cos{(\phi/2)} + \boldsymbol{n}\sin{(\phi/2)}$ is defined within the unit-quaternion group, $\mathrm{Spin}(3)$, in which $\phi \in [0, 2\pi)$ is the rotation angle around the rotation axis $\boldsymbol{n}$. Notice the rotation axis $\boldsymbol{n}$ is a unitary pure quaternion, that is, $\boldsymbol{n} \in \mathbb{H}_p \cap \mathbb{S}^3$ with $\mathbb{S}^3 = \{\boldsymbol{h} \in \mathbb{H} : \|\boldsymbol{h}\| = 1\}$. For further details of the unit-dual quaternion representation see [11, 35–39].

The set $\mathcal{H}_p = \{\underline{\boldsymbol{h}} \in \mathcal{H} : \mathrm{Re}\,(\underline{\boldsymbol{h}}) = 0\}$ of pure dual quaternions is used to represent twists and wrenches, which are represented in different coordinate systems using the adjoint operator $\mathrm{Ad} : \underline{\boldsymbol{\mathcal{S}}} \times \mathcal{H}_p \to \mathcal{H}_p$. For instance, consider the twist $\underline{\boldsymbol{\xi}}^a \in \mathcal{H}_p$ expressed in frame $\mathcal{F}_a$ and the unit dual quaternion $\underline{\boldsymbol{x}}_a^b$ that represents the rigid motion from $\mathcal{F}_b$ to $\mathcal{F}_a$. The same twist is expressed in frame $\mathcal{F}_b$ as

$$\underline{\boldsymbol{\xi}}^b = \mathrm{Ad}\left(\underline{\boldsymbol{x}}_a^b\right)\underline{\boldsymbol{\xi}}^a = \underline{\boldsymbol{x}}_a^b \underline{\boldsymbol{\xi}}^a \left(\underline{\boldsymbol{x}}_a^b\right)^*. \tag{2}$$

Furthermore, it is critical to highlight that from a differential geometry perspective, the Lie group associated to $\mathrm{Spin}(3) \ltimes \mathbb{R}^3$ is defined within a differentiable Riemannian manifold [40]. As a direct consequence, Riemannian metrics based on a collection of inner products on the tangent space at $\mathrm{Spin}(3) \ltimes \mathbb{R}^3$ can be assigned to the manifold [19, 40, 41]. These Riemannian metrics define the length of paths along the manifold [42], and therefore allow us to define minimum curve lengths, i.e., geodesics, see [41–44] for further information. In such manifolds, actions in the geodesics can be expressed by means of the exponential map $\exp_{\underline{\boldsymbol{x}}} : \mathcal{T}_{\underline{\boldsymbol{x}}}\mathrm{Spin}(3) \ltimes \mathbb{R}^3 \to \mathrm{Spin}(3) \ltimes \mathbb{R}^3$. The $\exp_{\underline{\boldsymbol{x}}}$ locally maps a vector in the tangent space $\mathcal{T}_{\underline{\boldsymbol{x}}}\mathrm{Spin}(3) \ltimes \mathbb{R}^3$ (at $\underline{\boldsymbol{x}} \in \mathrm{Spin}(3) \ltimes \mathbb{R}^3$)[2] to a point on the manifold following the geodesic through $\underline{\boldsymbol{x}}$ [45]. The inverse mapping (from manifold to tangent space at the point $\underline{\boldsymbol{x}}$) is the logarithm map $\log_{\underline{\boldsymbol{x}}} : \mathrm{Spin}(3) \ltimes \mathbb{R}^3 \to \mathcal{T}_{\underline{\boldsymbol{x}}}\mathrm{Spin}(3) \ltimes \mathbb{R}^3$.

The mappings $\exp_{\underline{\boldsymbol{x}}}$ and $\log_{\underline{\boldsymbol{x}}}$ are non-trivial to obtain. A solution is to compute them by parallel transport [40, 46]. The parallel transport exploits the exponential function that maps vectors from the tangent space (at the identity) to the manifold [43],

$$\begin{aligned}\exp_{\underline{\boldsymbol{x}}}(\underline{\boldsymbol{y}}) &= \underline{\boldsymbol{x}}\exp(\underline{\boldsymbol{x}}^*\underline{\boldsymbol{y}}), \\ \log_{\underline{\boldsymbol{x}}}(\underline{\boldsymbol{z}}) &= \underline{\boldsymbol{x}}\log(\underline{\boldsymbol{x}}^*\underline{\boldsymbol{z}}),\end{aligned} \tag{3}$$

where $\underline{\boldsymbol{z}} \in \mathrm{Spin}(3) \ltimes \mathbb{R}^3$ and $\underline{\boldsymbol{y}}$ is defined in the tangent space at $\underline{\boldsymbol{x}}$—notice that $\underline{\boldsymbol{y}}$ is not a unit DQ. The exp and log maps from the tangent space, at the identity, i.e., $\mathcal{T}_{\underline{\boldsymbol{1}}}\mathrm{Spin}(3) \ltimes \mathbb{R}^3$ are given by the dual vector representing the axis of screw motion and the dual angle containing both the translation length and the angle of rotation, see further details in [19, 25, 36, 40, 45, 47].

2.2   Overview of the Problem

In this work, we are interested in the design of a real-time motion planning solution that considers geometric constrains from prescribed keypoints in a

---

[2] The tangent space at $\underline{\boldsymbol{x}}$ is built by the collection of vectors whose inner products with $\underline{\boldsymbol{x}}$ is null—that is the orthogonal vector space to $\underline{\boldsymbol{x}}$.

coordinate-invariant fashion, while ensuring smooth movements and addressing twist, acceleration and jerk constraints in real-time. The proposed motion generation scheme takes as prior knowledge any n-number of keypoints in task-space,

$$\mathcal{K} = \{\underline{\boldsymbol{k}}_1, \underline{\boldsymbol{k}}_2, \ldots, \underline{\boldsymbol{k}}_\ell, \ldots \underline{\boldsymbol{k}}_n\}, \quad \underline{\boldsymbol{k}}_\ell \in \mathrm{Spin}(3) \ltimes \mathbb{R}^3. \tag{4}$$

These keypoints implicitly embed the desired task-space constraints and range. In this way, following a screw-linear interpolation, our planner also ensures that the resulting sequence of rigid body transformations from interpolation satisfies the observed task-space constraints in pose, i.e., orientation and translation as well. Notwithstanding, in case either the prescribed or resulting twists, acceleration or jerks are not feasible, the real-robot system would fail in deployment. To ensure additional constraint satisfaction, not only instantaneous, but rather along the trajectory, we propose a cascade approach with a model-predictive control system that takes the dual-quaternion algebra and the mapping to the tangent space of the prescribed poses in the path into account. This leads to a smooth motion planner satisfying the below problem definition.

Problem Definition: Given a set of n-number of keypoints in the task-space, $\mathcal{K}$, with $n \geq 2$, find a trajectory from $\underline{\boldsymbol{k}}_0$ to $\underline{\boldsymbol{k}}_n$ such that

1. The implicit constraints within $\mathcal{K}$ are satisfied as close as possible;
2. Motion generation is achieved in real-time with an additional constraint satisfaction and smooth motion regarding twists, acceleration and jerk constraints.

3 ScLERP-MPC: A Motion Planner based on Screw-linear Interpolation & Model-Predictive Control

This section presents an integrated screw-linear interpolation with a model-predictive control solution to address the problems designed in the problem definition. From the desired set of n keypoints in the task-space, $\mathcal{K}$, we first need an initial path planning structure going through along the desired setpoints.

The ScLERP [25] explores the screw-linear interpolation that connects any two points through the geodesic prescribed in the previous section. Given $\underline{\boldsymbol{x}}_a$ and $\underline{\boldsymbol{x}}_b$, the resulting path should be given by $\underline{\boldsymbol{x}}(\tau) : [0, 1] \to \mathrm{Spin}(3) \ltimes \mathbb{R}^3$ with $\underline{\boldsymbol{x}}(0) = \underline{\boldsymbol{x}}_a$ and $\underline{\boldsymbol{x}}(1) = \underline{\boldsymbol{x}}_b$. The process starts by mapping $\underline{\boldsymbol{x}}_b$ following the geodesic on $\mathrm{Spin}(3) \ltimes \mathbb{R}^3$ through $\underline{\boldsymbol{x}}_a$ onto the tangent space at $\underline{\boldsymbol{x}}_a$. In other words, it obtains a $\mathcal{T}_{\underline{\boldsymbol{x}}_a} \mathrm{Spin}(3) \ltimes \mathbb{R}^3$ corresponding to the geodesic direction of $\underline{\boldsymbol{x}}_b$ w.r.t. $\underline{\boldsymbol{x}}_a$. Hence,

$$\log_{\underline{\boldsymbol{x}}_a}(\underline{\boldsymbol{x}}_b) = \underline{\boldsymbol{x}}_a \log(\underline{\boldsymbol{x}}_a^* \underline{\boldsymbol{x}}_b), \tag{5}$$

where the mapping $\exp_{\underline{\boldsymbol{x}}_1}$ and $\log_{\underline{\boldsymbol{x}}_a}$ is computed using the parallel transport (3), and defines the tangent space of a Riemannian manifold—a vector space. From the geodesic path in the tangent space, one can linearly interpolate points from $\log_{\underline{\boldsymbol{x}}_a}(\underline{\boldsymbol{x}}_a)$ towards $\log_{\underline{\boldsymbol{x}}_a}(\underline{\boldsymbol{x}}_b)$, as $(\log_{\underline{\boldsymbol{x}}_a}(\underline{\boldsymbol{x}}_b) - \log_{\underline{\boldsymbol{x}}_a}(\underline{\boldsymbol{x}}_a))\tau + \log_{\underline{\boldsymbol{x}}_a}(\underline{\boldsymbol{x}}_a)$, with $\log_{\underline{\boldsymbol{x}}_a}(\underline{\boldsymbol{x}}_a)=0$. Hence, using the parallel transport (3) to map the vector in $\mathcal{T}_{\underline{\boldsymbol{x}}_a} \mathrm{Spin}(3) \ltimes \mathbb{R}^3$ back to the $\underline{\boldsymbol{\mathcal{S}}}$ manifold (following the geodesics along $\underline{\boldsymbol{x}}_a$) gives way to

$$\underline{\boldsymbol{x}}(\tau) = \exp_{\underline{\boldsymbol{x}}_a}\left(\underline{\boldsymbol{x}}_a \log(\underline{\boldsymbol{x}}_a^* \underline{\boldsymbol{x}}_b)\tau\right)$$

$$= \underline{\boldsymbol{x}}_a \exp\left(\log(\underline{\boldsymbol{x}}_a^* \underline{\boldsymbol{x}}_b)\tau\right). \tag{6}$$

Following (6), the prescribed discrete path linearly-scaled along the geodesic between two keypoints $\underline{\boldsymbol{x}}_a$ and $\underline{\boldsymbol{x}}_b$ can be derived as [25]

$$\underline{\boldsymbol{x}} = \text{ScLERP}(\underline{\boldsymbol{x}}_a, \underline{\boldsymbol{x}}_b; \tau) = \underline{\boldsymbol{x}}_a(\underline{\boldsymbol{x}}_a^{-1}\underline{\boldsymbol{x}}_b)^\tau, \tag{7}$$

with $\tau \in [0\ 1]$ defined within equally spaced values. Notice the ScLERP function (7) is the same as the one derived in (6). This can be shown by geometrical exponential [36, 48], and from the scaling of the dual rotation angle about the screw axis—hence the name [49]. Furthermore, the ScLERP interpolation allows for the coordinate-invariant interpolation which is not possible when decoupling orientation and translation [25, 50], as detailed in [24].[3]

The resulting screw interpolation can be used to connect all keypoints from (4). The resulting connected path from the coordinate-invariant ScLERP interpolation (7) through $\underline{\boldsymbol{k}}_\ell$ to $\underline{\boldsymbol{k}}_{\ell+1}$ within $\mathcal{K}$, $\ell = 1, \ldots, n-1$, results in a discrete set of desired poses $\underline{\boldsymbol{x}}_d$. The desired twist between the discrete points can be either user-defined or follow a C_0 path. In this case, the prescribed reference twist, $\underline{\boldsymbol{\xi}}_r \in \mathcal{H}_p$, is given in a way to describe the geodesic path within the given time-step i,

$$\underline{\boldsymbol{\xi}}_r[i] = \frac{2}{\tau}\log(x_d[i]x_d^*[i-1]). \tag{8}$$

Notwithstanding the result trajectory is C_0, and hence might not be feasible for the robot system to execute. Thus, for our framework we integrate a discrete MPC to improve smoothness and moreover ensure the twist, acceleration and jerk constraints in the task-space are satisfied. The discrete MPC optimizes the future control trajectory within the finite control horizon $n_c \in \mathbb{N}$ in the prediction horizon. To track the desired trajectory, we consider the system as a double integrator, that is $\boldsymbol{u}[i] = \text{vec}_6\left(\ddot{\underline{\boldsymbol{\xi}}}_r\right) \in \mathbb{R}^6$, in which the operator $\text{vec}_6 : \mathcal{H} \to \mathbb{R}^6$ maps the coefficients of a pure dual quaternion into a sixth-dimensional vector.[4] The state space equations are given by

$$\begin{bmatrix} \dot{\xi}_r[i] \\ \ddot{\xi}_r[i] \end{bmatrix} = \underbrace{\begin{bmatrix} \boldsymbol{0}_{6\times6} & \boldsymbol{I}_{6\times6} \\ \boldsymbol{0}_{6\times6} & \boldsymbol{0}_{6\times6} \end{bmatrix}}_{\boldsymbol{A}_m} \begin{bmatrix} \xi_r[i] \\ \dot{\xi}_r[i] \end{bmatrix} + \underbrace{\begin{bmatrix} \boldsymbol{0}_{6\times6} \\ \boldsymbol{I}_{6\times6} \end{bmatrix}}_{\boldsymbol{B}_m} \boldsymbol{u}[i],$$

$$\xi_{\text{eff}}[i] = \underbrace{\begin{bmatrix} \boldsymbol{I}_{6\times6} & \boldsymbol{0}_{6\times6} \end{bmatrix}}_{\boldsymbol{C}_m} \begin{bmatrix} \xi_{\text{eff}}[i] \\ \dot{\xi}_r[i] \end{bmatrix}, \tag{9}$$

---

[3] Similar interpolation scheme nonetheless could also be derived from $SE(3)$, and other covering groups that satisfy left-invariance and are based on non-minimal representation of rigid displacements. Hence, it is by no means restricted to the choice of $\text{Spin}(3) \ltimes \mathbb{R}^3$. Still, a matrix-based solution is non-attractive due to the additional computational cost—that can possibly restrict real-time implementation—and due to the efficiency, compactness and intuitiveness of $\text{Spin}(3) \ltimes \mathbb{R}^3$ which can depict wrenches, twists, geometric primitives, constraints and its tangent space with the same algebra.

[4] Given $\underline{\boldsymbol{h}} = \hat{\imath}h_2 + \hat{\jmath}h_3 + \hat{k}h_4 + \varepsilon\left(\hat{\imath}h_6 + \hat{\jmath}h_7 + \hat{k}h_8\right)$, $\text{vec}_6\,\underline{\boldsymbol{h}} = \begin{bmatrix} h_2 & \cdots & h_8 \end{bmatrix}^T$.

where $\dot{\xi}_{\text{eff}} = \text{vec}_6\left(\dot{\underline{\boldsymbol{\xi}}}_{\text{eff}}\right)$ and $\ddot{\xi}_{\text{eff}} = \text{vec}_6\left(\ddot{\underline{\boldsymbol{\xi}}}_{\text{eff}}\right)$ are, respectively, the first and the second order time derivatives of the end-effector twist and $\boldsymbol{I}_{6\times6}, \boldsymbol{0}_{6\times6} \in \mathbb{R}^{6\times6}$ are zero and identity matrices.

Applying the backward difference operator, the augmented state vector $\xi[i + 1] = \left[\Delta\Xi_{\text{r}}^T[i + 1]\,\xi_{\text{eff}}[i + 1]\right]^T \in \mathbb{R}^{18}$, with $\Delta\Xi[i+1] = \left[\Delta\xi_{\text{r}}[i + 1]\,\Delta\dot{\underline{\boldsymbol{\xi}}}_{\text{r}}[i + 1]\right]^T \in \mathbb{R}^{12}$, can be described by

$$\xi[i + 1] = \begin{bmatrix} \boldsymbol{A}_m & \boldsymbol{0}_{12\times6} \\ \boldsymbol{C}_m\boldsymbol{A}_m & \boldsymbol{I}_{6\times6} \end{bmatrix}[\xi[i]] + \begin{bmatrix} \boldsymbol{B}_m \\ \boldsymbol{C}_m\boldsymbol{B}_m \end{bmatrix}[\Delta\boldsymbol{u}[i]] \quad (10)$$

and also

$$\xi_{\text{eff}}[i] = \underbrace{\begin{bmatrix} \boldsymbol{0}_{6\times12} & \boldsymbol{I}_{6\times6} \end{bmatrix}}_{C}\begin{bmatrix} \Delta\Xi_{\text{r}} \\ \xi_{\text{eff}}[i] \end{bmatrix} \quad (11)$$

The control objective is to find the sequence of incremental control efforts $\Delta\boldsymbol{U}$ over the control horizon, defined as

$$\Delta\boldsymbol{U} = \left[\Delta\boldsymbol{u}^T[i]\,\,\Delta\boldsymbol{u}^T[i + 1]\,\,\cdots\,\,\Delta\boldsymbol{u}^T[i + n_c - 1]\right]^T, \quad (12)$$

such that $\Delta\boldsymbol{U} \in \mathbb{R}^{6n_c}$ is the solution of minimizing the formulation of the cost function based $\boldsymbol{L}$ on the Laguerre equations [51] taken as

$$\min_{\Delta\boldsymbol{U}} \boldsymbol{L}(\Delta\boldsymbol{U}) = \|\boldsymbol{\xi}_s - \boldsymbol{Y}\|_{Q_{\text{mpc}}} + \|\Delta\boldsymbol{U}\|_{R_{\text{mpc}}}, \quad (13)$$

subject to

$$\begin{cases} \dot{\boldsymbol{\vartheta}}_{min} \leq \Sigma\boldsymbol{U} \leq \dot{\boldsymbol{\vartheta}}_{max} \\ \ddot{\boldsymbol{\vartheta}}_{min} \leq \boldsymbol{U} \leq \ddot{\boldsymbol{\vartheta}}_{max} \\ \dddot{\boldsymbol{\vartheta}}_{min} \leq \Delta\boldsymbol{U} \leq \dddot{\boldsymbol{\vartheta}}_{max} \end{cases} \quad (14)$$

in which $\left[\dot{\boldsymbol{\vartheta}}_{min}\,\dot{\boldsymbol{\vartheta}}_{max}\right] \in \mathbb{R}^{12}$, $\left[\ddot{\boldsymbol{\vartheta}}_{min}\,\ddot{\boldsymbol{\vartheta}}_{max}\right] \in \mathbb{R}^{12}$, and $\left[\dddot{\boldsymbol{\vartheta}}_{min}\,\dddot{\boldsymbol{\vartheta}}_{max}\right] \in \mathbb{R}^{12}$ determine the limits in the Cartesian space for the admissible linear and angular velocities, accelerations, and jerks in the task pace respectively and $\boldsymbol{\xi}_s^T \in \mathbb{R}^{6\times n_p}$ is the vector that contains the information about the set points at the sampling time,

$$\boldsymbol{\xi}_s^T = \underbrace{\begin{bmatrix} 1 & 1 & \cdots & 1 \end{bmatrix}}_{n_p}\xi[i]. \quad (15)$$

The predicted output signal $\boldsymbol{Y}$ in the equation (13), which satisfies the boundary conditions on the upper and lower velocity, acceleration, and jerk bounds at the task space of the n-DoF manipulator, is the solution of (10) and (11), described as

$$\boldsymbol{Y} = \left[\xi_{\text{eff}}[i + 1|i]\,\,\xi_{\text{eff}}[i + 2|i]\,\,\cdots\,\,\xi_{\text{eff}}[i + n_p|i]\right] = \boldsymbol{F}\xi[i] + \phi\Delta\boldsymbol{U}, \quad (16)$$

where $\xi_{\text{eff}}[i + n_p|i]$ is the predicted twist at $i + n_p$ given the current plant information at sampling time i.

$$\boldsymbol{F} = \begin{bmatrix} CA\ CA^2\ CA^3 \cdots CA^{n_p} \end{bmatrix}^T \in \mathbb{R}^{6 \times (18 * n_p)},$$

$$\boldsymbol{\phi} = \begin{bmatrix} CB & O & O & \cdots & O \\ CAB & CB & O & \cdots & O \\ CA^2B & CAB & CB & \cdots & O \\ \vdots & \vdots & \vdots & \vdots & \vdots \\ CA^{n_p-1}B & CA^{n_p-2}B & CA^{n_p-3}B & \ldots & CA^{n_p-n_c}B \end{bmatrix} \in \mathbb{R}^{(6*n_p) \times (6*n_c)} \quad (17)$$

will result in a predicted sequence of the state vectors

$$\begin{bmatrix} \xi[i + 1|i]\ \xi[i + 2|i] \cdots \xi[i + n_p|i] \end{bmatrix}. \tag{18}$$

From (18), the smoothed desired pose is obtained by

$$\underline{\boldsymbol{x}}_d[i] = \exp\left(\frac{k\underline{\boldsymbol{\xi}}[i + 1]}{2}\right)\underline{\boldsymbol{x}}_d[i - 1], \tag{19}$$

k is the integration step.

Finally, the error between the current end-effector pose and the desired pose $\underline{\boldsymbol{x}}_d[i]$ is defined as

$$\underline{\boldsymbol{e}}[i + 1] = 1 - \underline{\boldsymbol{x}}_d^*[i + 1]\underline{\boldsymbol{x}}_{\text{eff}}[i]. \tag{20}$$

Defining $u_{\dot{q}} = \dot{\boldsymbol{q}}$, and taking into account (20), consider the following control law to ensure the closed-loop stability of the system [19]

$$u_{\dot{q}} = -(\bar{\boldsymbol{H}}_8\,(\underline{\boldsymbol{x}}_d[i])\,\boldsymbol{C}_8\boldsymbol{J})^\dagger \boldsymbol{K}\, \text{vec}_8\,(\underline{\boldsymbol{e}}[i + 1]) \tag{21}$$

where $\boldsymbol{K}$ is a positive definite gain matrix, $\bar{\boldsymbol{H}}_8 : \mathcal{H} \to \mathbb{R}^{8 \times 8}$ is the Hamilton operator, such that $\text{vec}_8\,(\underline{\boldsymbol{h}}_1\underline{\boldsymbol{h}}_2) = \bar{\boldsymbol{H}}_8\,(\underline{\boldsymbol{h}}_2)\,\text{vec}_8\,\underline{\boldsymbol{h}}_1$, and the matrix $\boldsymbol{C}_8 \in \mathbb{R}^{8 \times 8}$ is defined as $\boldsymbol{C}_8 \triangleq \text{diag}\left(\begin{bmatrix} 1\ -1\ -1\ -1\ 1\ -1\ -1\ -1 \end{bmatrix}\right)$ and $\boldsymbol{J} \in \mathbb{R}^{8 \times 7}$ is the geometric jacobian [34].

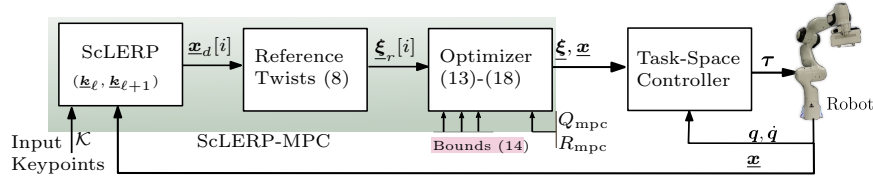Fig. 1 presents the conceptual block scheme of the overall proposed control architecture.

Fig. 1: Schematic block diagram of the ScLERP-MPC.

4   Experimental Results

To validate the proposed ScLERP-MPC formulation, we performed two sets of tests. In the first one, we performed simulations in CoppeliaSim [52] using a 7-DoF Franka Emika Robot to demonstrate the capabilities of the MPC on imposing the desired constraints. The second validation was done through experiments on the real platform.

4.1   Experimental setup

To get the solution of the cost function in equation (13), the following optimization problem is defined as the quadratic program given by

$$\min_{\Delta U} L(\Delta U) = \frac{1}{2}\Delta U^T(\phi^T Q_{mpc}\phi + R_{mpc})\Delta U + (\xi_s - F\xi)Q_{mpc}\Delta U \quad (22)$$

subject to,

$$W\Delta U \leq V, \quad (23)$$

where

$$W = \begin{bmatrix} W_1 \ W_2 \ W_3 \end{bmatrix}^T,$$

in which

$$W_1 = W_2 = W_3 = \begin{bmatrix} -I & 0 & 0 & \cdots & 0 & 0 \\ I & 0 & 0 & \cdots & 0 & 0 \\ 0 & I & 0 & \cdots & 0 & 0 \\ 0 & -I & 0 & \cdots & 0 & 0 \\ \vdots & \vdots & \vdots & \cdots & \vdots & \vdots \\ 0 & 0 & 0 & \cdots & 0 & -I \\ 0 & 0 & 0 & \cdots & 0 & I \end{bmatrix} \in \mathbb{R}^{12n_c \times 6n_c}$$

$I, O \in \mathbb{R}^{6 \times 6}$ are the identity and zero matrix respectively, and

$$V = \begin{bmatrix} V_1 \ V_2 \ V_3 \end{bmatrix}^T,$$

in which,

$$V_1 = \begin{bmatrix} -\dddot{\vartheta}_{min} \ \dddot{\vartheta}_{max} -\dddot{\vartheta}_{min} \ \dddot{\vartheta}_{max} \ldots -\dddot{\vartheta}_{min} \ \dddot{\vartheta}_{max} \end{bmatrix}^T \in \mathbb{R}^{12n_c},$$

$$V_2 = \begin{bmatrix} -\ddot{\vartheta}_{min} \ \ddot{\vartheta}_{max} -\ddot{\vartheta}_{min} \ \ddot{\vartheta}_{max} \ldots -\ddot{\vartheta}_{min} \ \ddot{\vartheta}_{max} \end{bmatrix}^T$$
$$\qquad - W_2 \begin{bmatrix} \ddot{\vartheta}[i-1] \ \ddot{\vartheta}[i-1] \ \ddot{\vartheta}[i-1] \ \ddot{\vartheta}[i-1] \ldots \ddot{\vartheta}[i-1] \ \ddot{\vartheta}[i-1] \end{bmatrix}^T \in \mathbb{R}^{12n_c},$$

$$V_3 = \begin{bmatrix} \phi^\dagger(-\dot{\vartheta}_{min} + F\xi[i]) \ \phi^\dagger(\dot{\vartheta}_{max} - F\xi[i]) \end{bmatrix}$$
$$\qquad\qquad \ldots \phi^\dagger(-\dot{\vartheta}_{min} + F\xi[i]) \ \phi^\dagger(\dot{\vartheta}_{max} - F\xi[i]) \end{bmatrix} \in \mathbb{R}^{12n_c}.$$

Furthermore, the upper and lower jerk, acceleration, and velocity constraints were selected to respect the limits of the Franka Emika Panda.[5]

The control horizon was chosen as $n_c = 10$, and the prediction range as $n_p = 50$. The stop criteria for the tests was $\underline{e} \leq$ tol, with tol $\in \mathbb{R}$ empirically defined. For the experiments on the real platform, the sampling rate for the MPC controller was $9ms$ while the low level controller was running at $1kHz$.

---

[5] https://frankaemika.github.io/docs/control_parameters.html

4.2   Simulations

For the simulations, we selected an interpolated trajectory that would intentionally force the robot outside the desired constraints to demonstrate that the proposed ScLERP-MPC formulation can ensure their enforcement.

Fig. 3 presents the end-effector twists, whereas Fig. 2 shows the angular and linear components of the end-effector pose. We can see that the executed trajectory presents a delay since the robot cannot violate the constraints of accelerations, and jerks. This behaviour is also observed in the resulting trajectory, Fig. 2.
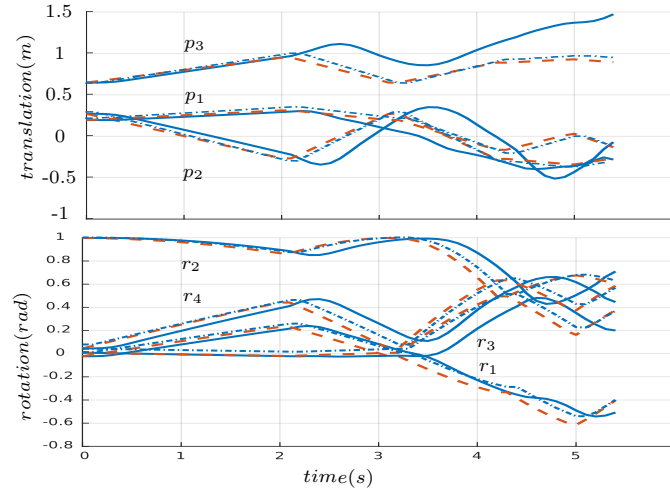
Fig. 2: Trajectories for the simulated scenario. *Solid blue* curves correspond to the SCLERP-MPC resulting trajectory whereas *Dashed blue* correspond a system without kinodynamic constraints. The *Dashed red* curves refer to the reference.
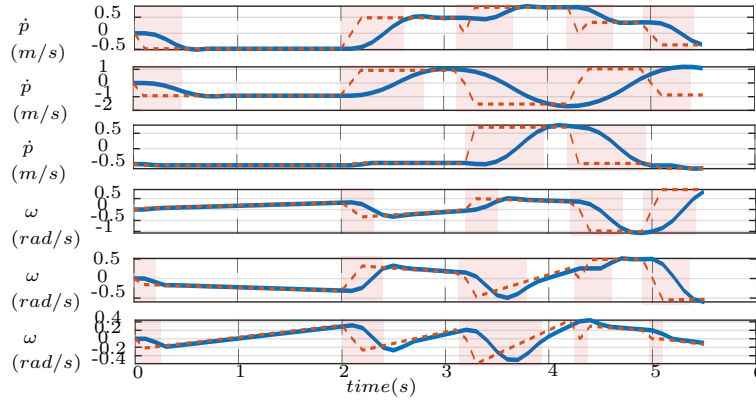
Fig. 3: Twist trajectory for the simulation scenario. *Solid blue* curves correspond to the SCLERP-MPC resulting trajectory whereas the *Dashed red* curves refer to the reference. The shadowed areas depict picks of acceleration and jerk above the robot limits.
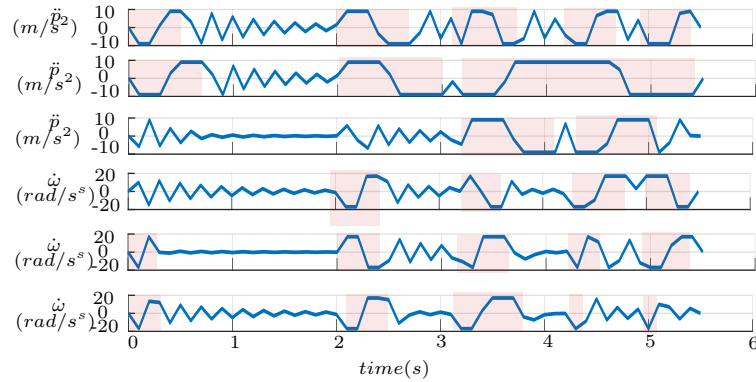
Fig. 4: Acceleration trajectory for the simulation scenario. *Solid blue* curves correspond to the SCLERP-MPC resulting trajectory. The shadowed areas depict picks of acceleration and jerk above the robot limits.

4.3 Experiments

For the experiments, the robot followed a trajectory obtained through the ScLERP method given two used-defined initial and final end-effector poses. The constraints imposed in the jerks, accelerations, and velocities followed the manufacturer recommendations to ensure safety of operation.

Fig.5 and Fig. 6 present the translation and rotation components of the pose, and angular and linear components of the end-effector twists successfully tracking the desired twist trajectory.
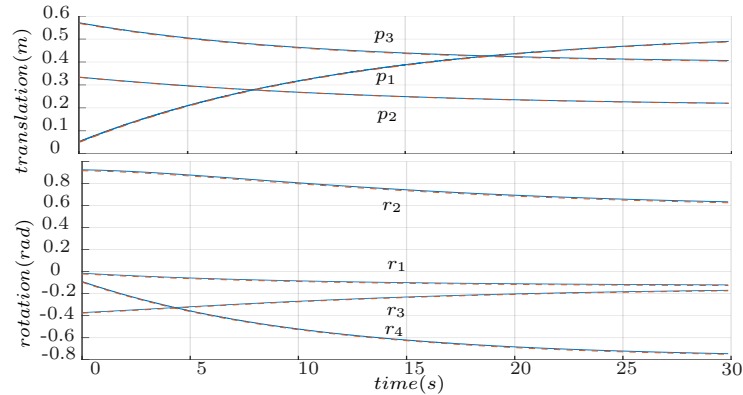

Fig. 5: Real-world experiment trajectories with SCLERP-MPC. *Solid blue* curves correspond to measured output, whereas the *Dashed red* refers to the reference.

5 Conclusions and Future Works

This paper presented a cascade structure for the tracking of a smooth coordinate-invariant trajectory using dual quaternion algebra. The proposed architecture integrates a screw-interpolation strategy that satisfies path and geometric constraints within a coordinate-invariant manner with a dual-quaternion algebra MPC that imposes the task-space constraints. The outer-loop MPC
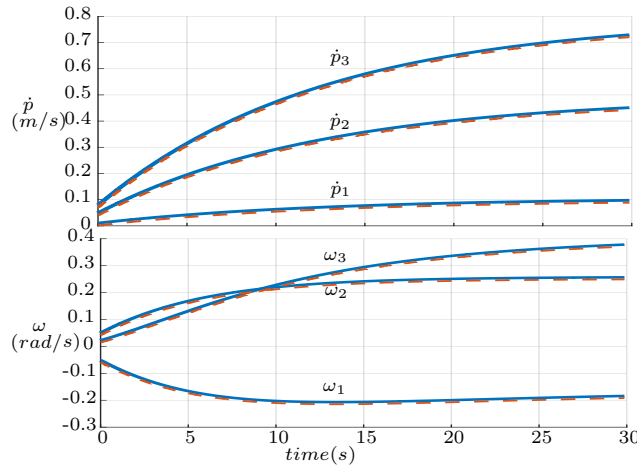
Fig. 6: Linear and angular components of the end-effector twist for the experiment performed on the real platform. *Solid blue* curves correspond to the values read from the robot, whereas *dashed red* curves to the reference.

performs real-time smoothing of the manipulator's end-effector twist while an inner-loop kinematic controller ensures tracking of the instantaneous desired end-effector pose.

Experiments on a 7-DoF Franka Emika Panda robotic manipulator have validated the proposed method demonstrating its application to constraint the robot twists, accelerations and jerks within prescribed bounds.

Future works will extend the proposed structure to robot dynamics as well as considerate the inclusion of variable impedance constraints.

References

1. O. Khatib, *The Potential Field Approach And Operational Space Formulation In Robot Control*, K. S. Narendra, Ed. Boston, MA: Springer US, 1986. [Online]. Available: http://link.springer.com/10.1007/978-1-4757-1895-9

2. M. M. Marinho, B. V. Adorno, K. Harada, and M. Mitsuishi, "Active Constraints Using Vector Field Inequalities for Surgical Robots," in *2018 IEEE International Conference on Robotics and Automation (ICRA)*. IEEE, May 2018, pp. 5364–5371. [Online]. Available: https://ieeexplore.ieee.org/document/8461105/

3. ——, "Dynamic Active Constraints for Surgical Robots Using Vector-Field Inequalities," *IEEE Transactions on Robotics*, vol. 35, no. 5, pp. 1166–1185, Oct. 2019. [Online]. Available: http://arxiv.org/abs/1804.11270

4. R. J. Kirschner, H. Mayer, L. Burr, N. Mansfeld, S. Abdolshah, and S. Haddadin, "Expectable motion unit: Avoiding hazards from human involuntary motions in human-robot interaction," *IEEE Robotics and Automation Letters*, vol. 7, no. 2, pp. 2993–3000, 2022.

5. F. M. Dimentberg, *Screw Theory and Its Application in Mechanics*, I. Nauka and G. Redaktsiya, Eds. Moskva: Fiziko-Matematicheskoy Literatury, 1965.

6. K. Waldron, "A method of studying joint geometry," *Mechanism and Machine Theory*, vol. 7, no. 3, pp. 347–353, Sep. 1972. [Online]. Available: https://linkinghub.elsevier.com/retrieve/pii/0094114X72900432

7. O. P. Agrawal, "Hamilton operators and dual-number-quaternions in spatial kinematics," *Mechanism and Machine Theory*, vol. 22, no. 6, pp. 569–575, Jan. 1987. [Online]. Available: https://linkinghub.elsevier.com/retrieve/pii/0094114X87900528

8. R. M. Murray, Z. Li, and S. S. Sastry, *A Mathematical Introduction to Robotic Manipulation.* CRC Press, 1994.

9. G. R. Pennock and B. A. Oncu, "Application of Screw Theory to Rigid Body Dynamics," *Journal of Dynamic Systems, Measurement, and Control*, vol. 114, no. 2, p. 262, 1992. [Online]. Available: http://dynamicsystems.asmedigitalcollection.asme.org/article.aspx?articleid=1405915

10. K. Wohlhart, "Motor Tensor Calculus," in *Angewandte Chemie International Edition, 6(11), 951-952.*, 1995, pp. 93–102.

11. N. A. Aspragathos and J. K. Dimitros, "A comparative study of three methods for robot kinematics," *IEEE Transactions on Systems, Man, and Cybernetics, Part B: Cybernetics*, vol. 28, no. 2, pp. 135–145, 1998.

12. J. M. Selig, "Lie Groups and Lie Algebras in Robotics," in *Computational Non-commutative Algebra and Applications.* Dordrecht, Netherlands: Kluwer Academic Publishers, 2004, pp. 101–125.

13. A. Cibicik and O. Egeland, "Kinematics and Dynamics of Flexible Robotic Manipulators Using Dual Screws," *IEEE Transactions on Robotics*, vol. 37, no. 1, pp. 206–224, Feb. 2021. [Online]. Available: https://ieeexplore.ieee.org/document/9174656/

14. A. Müller and S. Kumar, "Closed-form time derivatives of the equations of motion of rigid body systems," *Multibody System Dynamics*, Jul. 2021. [Online]. Available: http://dx.doi.org/10.1007/s11044-021-09796-8

15. F. F. A. Silva, J. J. Quiroz-Omaña, and B. V. Adorno, "Dynamics of Mobile Manipulators using Dual Quaternion Algebra," *Journal of Mechanisms and Robotics*, vol. 14, no. 6, p. 11, Jan. 2022. [Online]. Available: https://arxiv.org/abs/2007.08444

16. L. F. C. Figueredo, B. V. Adorno, and J. Y. Ishihara, "Robust h∞ kinematic control of manipulator robots using dual quaternion algebra," *Automatica*, vol. 132, p. 109817, 2021.

17. Q. J. Ge and B. Ravani, "Geometric Construction of Be´zier Motions," *Journal of Mechanical Design*, vol. 116, no. 3, pp. 749–755, Sep. 1994. [Online]. Available: https://asmedigitalcollection.asme.org/mechanicaldesign/article/116/3/749/454514/Geometric-Construction-of-Bezier-Motions

18. M. Vochten, T. De Laet, and J. De Schutter, "Comparison of rigid body motion trajectory descriptors for motion representation and recognition," in *2015 IEEE International Conference on Robotics and Automation (ICRA)*. Seattle, WA, USA: IEEE, May 2015, pp. 3010–3017. [Online]. Available: http://ieeexplore.ieee.org/document/7139612/

19. R. Laha, R. Sun, W. Wu, D. Mahalingam, N. Chakraborty, L. F. Figueredo, and S. Haddadin, "Coordinate invariant user-guided constrained path planning with reactive rapidly expanding plane-oriented escaping trees," in *2022 International Conference on Robotics and Automation (ICRA)*. IEEE, 2022, pp. 977–984.

20. C. Liu, S. Lee, S. Varnhagen, and H. E. Tseng, "Path planning for autonomous vehicles using model predictive control," in *2017 IEEE Intelligent Vehicles Symposium (IV)*. IEEE, 2017, pp. 174–179.

21. S. Schaal, J. Peters, J. Nakanishi, and A. Ijspeert, "Control, planning, learning, and imitation with dynamic movement primitives," in *Workshop on Bilateral Paradigms on Humans and Humanoids: IEEE International Conference on Intelligent Robots and Systems (IROS 2003)*, 2003, pp. 1–21.
22. S. Haddadin, R. Belder, and A. Albu-Schäffer, "Dynamic motion planning for robots in partially unknown environments," *IFAC Proceedings Volumes*, vol. 44, no. 1, pp. 6842–6850, 2011.
23. R. Laha, L. F. Figueredo, J. Vrabel, A. Swikir, and S. Haddadin, "Reactive Cooperative Manipulation based on Set Primitives and Circular Fields," in *IEEE International Conference on Robotics and Automation*, Xi'an, China, May 2021.
24. F. Allmendinger, S. Charaf Eddine, and B. Corves, "Coordinate-invariant rigid-body interpolation on a parametric C1 dual quaternion curve," *Mechanism and Machine Theory*, pp. 731–744, March 2018.
25. A. Sarker, A. Sinha, and N. Chakraborty, "On screw linear interpolation for point-to-point path planning," in *2020 IEEE/RSJ International Conference on Intelligent Robots and Systems (IROS)*. IEEE, 2020, pp. 9480–9487.
26. R. Laha, A. Rao, L. Figueredo, Q. Chang, S. Haddadin, and N. Chakraborty, "Point-to-point path planning based on user guidance and screw linear interpolation," in *Proceedings of the ASME International Design Engineering Technical Conferences and Computers and Information in Engineering Conference (IDETC/CIE)*, August 2021.
27. Y.-n. Fei and Q.-h. Wu, "Tracking control of robot manipulators via output feedback linearization," *Frontiers of Mechanical Engineering in China*, vol. 1, pp. 329–335, 2006.
28. E. Todorov *et al.*, "Optimal control theory," *Bayesian brain: probabilistic approaches to neural coding*, pp. 268–298, 2006.
29. D. Q. Mayne, J. B. Rawlings, C. V. Rao, and P. O. Scokaert, "Constrained model predictive control: Stability and optimality," *Automatica*, vol. 36, no. 6, pp. 789–814, 2000.
30. J. C. Pereira, V. J. Leite, and G. V. Raffo, "Nonlinear model predictive control on SE (3) for quadrotor aggressive maneuvers," *Journal of Intelligent & Robotic Systems*, vol. 101, pp. 1–15, 2021.
31. M. Kamel, M. Burri, and R. Siegwart, "Linear vs nonlinear MPC for trajectory tracking applied to rotary wing micro aerial vehicles," *IFAC-PapersOnLine*, vol. 50, no. 1, pp. 3463–3469, 2017.
32. A. Ferramosca, D. Limón, I. Alvarado, T. Alamo, and E. F. Camacho, "MPC for tracking with optimal closed-loop performance," in *2008 47th IEEE Conference on Decision and Control*. IEEE, 2008, pp. 4055–4060.
33. C. V. Rao and J. B. Rawlings, "Steady states and constraints in model predictive control," *AIChE Journal*, vol. 45, no. 6, pp. 1266–1278, 1999.
34. B. V. Adorno, "Two-arm Manipulation: From Manipulators to Enhanced Human-Robot Collaboration [Contribution à la manipulation à deux bras : des manipulateurs à la collaboration homme-robot]," Ph.D. dissertation, 2011.
35. J. M. Selig, *Geometric Fundamentals of Robotics*, D. Gries and F. B. Schneider, Eds. New York, NY: Springer New York, 2005.
36. B. V. Adorno, "Robot kinematic modeling and control based on dual quaternion algebra—part i: Fundamentals." 2017.

37. B. V. A, "Two-arm manipulation: From manipulators to enhanced human-robot collaboration," Ph.D. dissertation, Laboratoire d'Informatique, de Robotique et de Microélectronique de Montpellier (LIRMM) - Université Montpellier 2, Montpellier, France, 2011.

38. L. F. C. Figueredo, "Kinematic control based on dual quaternion algebra and its application to robot manipulators," Ph.D. dissertation, University of Brasilia, Brazil, 2016.

39. F. F. A. Silva, "Dynamic Modeling of Robotic Systems: A Dual Quaternion Formulation," Ph.D. dissertation, Federal University of Minas Gerais, Minas Gerais, Brazil, Jun. 2022. [Online]. Available: http://hdl.handle.net/1843/46591

40. B. Busam, T. Birdal, and N. Navab, "Camera pose filtering with local regression geodesics on the riemannian manifold of dual quaternions," in *2017 IEEE International Conference on Computer Vision (ICCV)*, 2017, pp. 2436–2445.

41. W. M. Boothby, *An Introduction to Differentiable Manifolds and Riemannian Geometry*, 2nd ed. Academic Press, 2002.

42. F. C. Park, "Distance Metrics on the Rigid-Body Motions with Applications to Mechanism Design," *Journal of Mechanical Design – Transactions of ASME*, vol. 117, no. 1, pp. 48–54, 1995.

43. E. Zacur, M. Bossa, and S. Olmos, "Left-Invariant Riemannian Geodesics on Spatial Transformation Groups," *SIAM Journal on Imaging Sciences*, vol. 7, no. 3, pp. 1503–1557, jul 2014.

44. Y. L. Sachkov, "Control theory on Lie groups," *Journal of Mathematical Sciences*, vol. 156, no. 3, pp. 381–439, 2009.

45. B. Busam, T. Birdal, and N. Navab, "Camera Pose Filtering with Local Regression Geodesics on the Riemannian Manifold of Dual Quaternions," *ArXiv e-prints*, 2017. [Online]. Available: http://arxiv.org/abs/1704.07072

46. M. Lorenzi and X. Pennec, "Geodesics, parallel transport & one-parameter subgroups for diffeomorphic image registration," *International Journal of Computer Vision*, vol. 105, pp. 111–127, 2013.

47. X. Wang, D. Han, C. Yu, and Z. Zheng, "The geometric structure of unit dual quaternion with application in kinematic control," *Journal of Mathematical Analysis and Applications*, vol. 389, no. 2, pp. 1352–1364, May 2012.

48. M.-j. Kim, M.-s. Kim, and S. Y. Shin, "A compact differential formula for the first derivative of a unit quaternion curve," *The Journal of Visualization and Computer Animation*, vol. 7, no. 1, pp. 43–57, 1996.

49. L. Kavan, S. Collins, C. O'Sullivan, and J. Zara, "Dual quaternions for rigid transformation blending," Trinity College Dublin, Tech. Rep., Trinity College Dublin 2006.

50. R. Grassmann, L. Johannsmeier, and S. Haddadin, "Smooth point-to-point trajectory planning in $SE(3)$ with self-collision and joint constraints avoidance," in *2018 IEEE/RSJ International Conference on Intelligent Robots and Systems (IROS)*. IEEE, 2018, pp. 1–9.

51. L. Wang, *Model predictive control system design and implementation using MATLAB®*. Springer Science & Business Media, 2009.

52. E. Rohmer, S. P. Singh, and M. Freese, "V-rep: A versatile and scalable robot simulation framework," in *2013 IEEE/RSJ international conference on intelligent robots and systems*. IEEE, 2013, pp. 1321–1326.